



Probing the exciton condensate via shot noise spectroscopy in superconducting hybrid structures based on excitonic insulators

Biao Wu and Hai Li ^{*}

Key Laboratory of Low-Dimensional Quantum Structures and Quantum Control of Ministry of Education, Key Laboratory for Matter Microstructure and Function of Hunan Province, School of Physics and Electronics, Hunan Normal University, Changsha 410081, China

 (Received 18 December 2023; revised 6 February 2024; accepted 16 February 2024; published 1 March 2024)

We theoretically study the shot noise and the Fano factor in a voltage-biased junction consisting of a bilayer excitonic insulator (EI) sandwiched between a bilayer semimetal (SM) and a conventional superconductor (S). By comparing the scenarios in SM-EI-S junctions with and without exciton condensates, we illustrate the effects of exciton condensates on the shot noise and demonstrate that the shot noise spectroscopy can signify the existence of exciton condensate in both well-contacted and tunnel SM-EI-S junctions. We also show that in a tunnel SM-EI-S junction, the Fano factor located in the super-Poissonian regime is a consequence of the competition between the exciton-mediated normal reflection and the Cooper-pair-mediated Andreev reflection. By virtue of the scattering probabilities, we elucidate the underlying physics. These results offer an alternative route toward the identification of neutral exciton condensate via charge transport measurements.

DOI: [10.1103/PhysRevB.109.125402](https://doi.org/10.1103/PhysRevB.109.125402)

I. INTRODUCTION

The excitonic insulator (EI) arises from the condensate of electron-hole pairs bound by Coulomb attraction in a narrow-gap semiconductor or a small band-overlap semimetal (SM) [1–3]. During the last decade, experimental indications of this excitonic ordered state have been proposed in a series of candidate materials including 1T-TiSe₂ [4], Ta₂NiSe₅ [5,6], WTe₂ monolayer [7,8], and MoSe₂-WSe₂ double layers [9,10]. Spurred in part by the tremendous progress in the synthesis of various layered materials, the list of EI candidates is rapidly updating, thereby boosting the research activities to detect and engineer novel states in EIs and EI-based hybrid structures [11–20].

The exciton condensate in semimetallic systems can be characterized in analogy with the Bardeen-Cooper-Schrieffer (BCS) theory of superconductivity [1,2]. In the framework of the BCS-like picture, the coherent transport related to the exciton condensate has been intensively investigated in EI-based hybrid structures [21–33]. A particularly prominent example is the prediction of the electrical signature of neutral exciton condensate in a junction consisting of a bilayer EI sandwiched between a bilayer SM and a conventional superconductor (S) [26,27]. Owing to the interplay between neutral excitons and charged Cooper pairs, in a SM-EI-S junction with high transparency, the exciton-mediated normal reflection (NR) dominates over the Cooper-pair-mediated Andreev reflection (AR) when the incident energy E is less than the excitonic gap Γ . As a consequence, the differential conductance exhibits a minimum at $E \simeq \Gamma$, which can serve as a direct hallmark for detecting the exciton condensate in a well-contacted SM-EI-S junction [26,27]. In a parallel vein, the phase

controllable conversion between the neutral exciton flow and the charged supercurrent has been theoretically demonstrated in bilayer-EI-based Josephson junctions, holding the promise for probing the neutral exciton condensate in terms of charge transport measurements [29,30].

While substantial efforts have been devoted to unveiling the effects of exciton condensates on the charge transport properties of EI-based superconducting hybrid structures, the research attention to date has been restricted to the time-averaged quantities such as the differential conductance [26–28] and current [29,30]. In contrast, the manifestations of the interplay between neutral excitons and charged Cooper pairs in the nonequilibrium current fluctuations have been scarcely studied in EI-based superconducting hybrid structures. As it is commonly known, the signatures intrinsic to the nonequilibrium current fluctuations can provide information on the nature of transport that are not accessible through the current and conductance measurements [34–48]. In the present paper, we address this issue in a SM-EI-S junction resorting to the shot noise spectroscopy.

Shot noise refers to the nonequilibrium fluctuations of currents emanating from the discreteness of carriers and the stochastic nature of scattering processes [43–46]. The shot noise spectroscopy has been employed to decipher the degree of correlations and the effective charge of carriers in a variety of hybrid heterostructures, including normal-metal-superconductor (NS) junctions [41–49] and N-EI junctions [31–33]. In a low transparent NS junction with the bias voltage below the superconducting gap Δ , the shot noise is doubled as compared to the case of a corresponding NN junction, due to the AR process by which an effective charge of $2e$ is transferred [45–52], while the shot noise in a N-EI junction vanishes in the regime of $0 < E < \Gamma$, since the exciton blockade effect completely suppresses the transmission of quasiparticles and leads to nonrandom scattering

^{*}hnnuhl@hunnu.edu.cn

[21,22,31–33]. Under these lines, it is natural to ask that in a SM-EI-S junction with both exciton and superconducting condensates, how does the interplay between the neutral excitons and charged Cooper pairs affect the shot noise? On the other hand, we note that in a well-contacted SM-EI-S junction, the hallmark of exciton condensate proposed in Refs. [26,27] is encoded in the minimum of differential conductance located within the subgap regime of $0 < E < \Delta$. However, in a tunnel SM-EI-S junction, the differential conductance almost vanishes in the whole subgap regime of $0 < E < \Delta$ [51], thus smearing the signature of the minimal differential conductance caused by the exciton-mediated scattering. As such, the subgap differential conductance may be incapable of directly proving the existence of exciton condensates in a tunnel SM-EI-S junction. In order to extend the proposal on the charge transport measurements of neutral exciton condensates to the situation of a tunnel SM-EI-S junction, it is highly desirable to provide an alternative route to pinpoint the exciton-mediated scattering scenarios.

In this paper, we study the nonequilibrium current fluctuations in SM-EI-S junctions by calculating the differential shot noise and the Fano factor. By comparing the E -dependent differential shot noise in the SM-EI-S junctions with and without exciton condensates, we illustrate the influences of exciton-mediated scattering on the differential shot noise. We demonstrate that the shot noise spectroscopy can serve as a hallmark to testify the existence of exciton condensate in both well-contacted and tunnel SM-EI-S junctions, thus extending the previous proposals on the charge transport measurements of exciton condensates [26,27] to the situations of tunnel SM-EI-S junctions. Furthermore, we show that in a tunnel SM-EI-S junction the value of Fano factor lies within the super-Poissonian regime when $\Gamma < eV < \Delta$ with V the bias voltage. This scenario results from the energy-dependent competition between the exciton-mediated interlayer NR and the Cooper-pair-mediated intralayer AR, which can profoundly modify the transparency of the EI region. Resorting to the scattering probabilities, we explicitly elucidate the underlying mechanism. These results provide an alternative route to probe the neutral exciton condensate in bilayer systems.

The paper is organized as follows. We present the model and calculation method in Sec. II. In Sec. III, we give the numerical results and discuss the manifestations of the interplay between the neutral excitons and charge Cooper pairs in the shot noise and the Fano factor. Finally, we summarize the results and draw a brief conclusion in Sec. IV.

II. MODEL AND METHOD

We consider a setup similar to the one proposed in Ref. [26]. As schematically shown in Fig. 1, a bilayer EI is placed in the xy plane, with two metallic electrodes and two superconducting electrodes covering the regions of $x < 0$ and $x > L$, respectively. The Coulomb interaction between the top (T) and bottom (B) layers is assumed to be screened by the metallic electrodes, so that the region of $x < 0$ can be modeled by a two-band SM [26]. In the $x > L$ region, the superconductivity is induced by the superconducting electrodes via the proximity effect [26,29,30,52]. The Bogoliubov-de Gennes (BdG) Hamiltonian describing the SM-EI-S junction

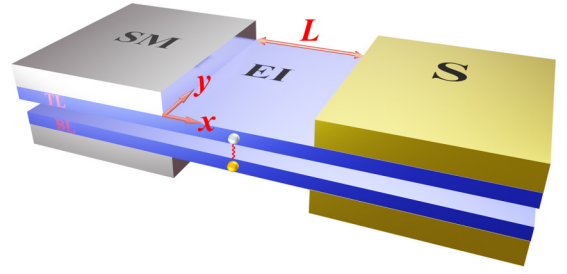


FIG. 1. Schematic of a junction consisting of a bilayer excitonic insulator (EI) sandwiched between a bilayer semimetal (SM) and a conventional superconductor (S), where a bilayer EI is in contact, respectively, with two metallic electrodes covering the region of $x < 0$ and two superconducting electrodes depositing in the region of $x > L$. The transport along the x direction is concerned.

takes the form of $H_{\text{BdG}} = \int_{-\infty}^{\infty} dx \hat{\Psi}^\dagger(x) \mathcal{H} \hat{\Psi}(x)$ [26,29,30], where $\hat{\Psi}^\dagger = (\Psi_{T,\uparrow}^\dagger, \Psi_{B,\uparrow}^\dagger, \Psi_{T,\downarrow}, \Psi_{B,\downarrow})$ spanned in the Nambu \otimes sublayer space, and

$$\mathcal{H} = \tau_z \otimes \left[\left(-\frac{\hbar^2 \partial_x^2}{2m} - \mathcal{E} \right) \sigma_z + \Gamma(x) \sigma_x \right] + \Delta(x) \tau_x \otimes \sigma_0, \quad (1)$$

with $\sigma_{x,z}$ ($\tau_{x,z}$) the Pauli matrices operating in the sublayer (Nambu) subspace, and σ_0 a 2×2 unit matrix. The overlap between the bands of the T and B layers is parametrized as \mathcal{E} , which can be modulated by gating the two layers independently [26,29,30]. Following Refs. [26,27,29,30], we assume that the superconducting order parameter $\Delta(x)$ and the exciton condensate order parameter $\Gamma(x)$ can be effectively characterized by step functions, i.e., $\Delta(x) = \Delta \Theta(x - L)$ and $\Gamma(x) = \Gamma \Theta(x) \Theta(L - x)$, with $\Theta(x)$ the Heaviside step function.

In the present work, we study the shot noise in terms of the scattering wave approach. This method has been extensively employed to investigate the transport properties in various hybrid heterostructures with arbitrary transparency [26,27,30,42–46]. We focus on the transport scenarios caused by an incident electron stemming from the T layer of the SM region. Owing to simultaneous occurrence of the exciton-mediated intralayer scattering and the Cooper-pair-mediated Andreev scattering, there exist four possible reflection processes. Specifically, the incident electron originating from the T layer of the SM region can either be normally reflected back as an electron into the T (B) layer with amplitude r_{ee}^{TT} (r_{ee}^{BT}), or be Andreev-reflected back as a hole into the T (B) layer with amplitude r_{he}^{TT} (r_{he}^{BT}). Hence, in the SM region ($x < 0$) the resulting wave function Ψ_{SM} is given by

$$\Psi_{\text{SM}} = \psi_{\text{SM},e}^{\text{T},+} + \sum_{\alpha=\text{T},\text{B}} \sum_{q=e,h} r_{qe}^{\alpha\text{T}} \psi_{\text{SM},q}^{\alpha,-}. \quad (2)$$

The basis scattering states $\psi_{\text{SM},e(h)}^{\text{T(B)},\pm}$ and $\psi_{\text{SM},e(h)}^{\text{B(T)},-}$ can be obtained by solving the BdG equation $\mathcal{H}\psi = E\psi$ straightforwardly, and the details are presented in Eq. (A1). On the other hand, the incident electron can tunnel into the T (B) layer of the S region ($x > L$) as an electronlike quasiparticle with amplitude t_{ee}^{TT} (t_{ee}^{BT}) or as a holelike quasiparticle with amplitude t_{he}^{TT} (t_{he}^{BT}). Consequently, in the S region the wave

function Ψ_S can be written as

$$\Psi_S = \sum_{\alpha=T,B} \sum_{q=\tilde{e},\tilde{h}} t_{qe}^{\alpha T} \psi_{S,q}^{\alpha,+}, \quad (3)$$

where the electronlike (holelike) quasiparticle is denoted by the index $q = \tilde{e}(\tilde{h})$, and the basis scattering states $\psi_{S,\tilde{e}(\tilde{h})}^{T(B),+}$ and $\psi_{S,\tilde{e}(\tilde{h})}^{B(T),+}$ are given by Eq. (A2). In the EI region ($0 < x < L$), the wave function Ψ_{EI} is a linear combination of all possible scattering states, i.e.,

$$\Psi_{EI} = \sum_{\alpha=T,B} \sum_{q=e,h} (c_q^\alpha \psi_{EI,q}^{\alpha,+} + d_q^\alpha \psi_{EI,q}^{\alpha,-}), \quad (4)$$

where the related scattering amplitudes are indicated by c_q^α and d_q^α , and the basis scattering states $\psi_{EI,e}^{T(B),\pm}$ and $\psi_{EI,h}^{T(B),\pm}$ are shown in Eq. (A3).

In general, at the boundaries of $x = 0$ and $x = L$ there inevitably exist interfacial imperfections caused by the electrodes. In order to capture the essential effects of the interfacial imperfections on the transport properties, we introduce two interfacial potential barriers characterized by $U(x) = Z_1 \hbar^2 k_0^2 / (2m) \delta(x) + Z_2 \hbar^2 k_0^2 / (2m) \delta(x - L)$, where $Z_{1(2)}$ denotes the dimensionless strength of the interfacial potential barrier located at $x = 0$ ($x = L$), $\delta(x)$ labels the Delta function, and $k_0 = \sqrt{2m\mathcal{E}/\hbar^2}$. In doing so, the boundary conditions can be formulated as

$$\Psi_{SM}|_{x=0^-} = \Psi_{EI}|_{x=0^+}, \quad (5a)$$

$$\Psi_{EI}|_{x=L^-} = \Psi_S|_{x=L^+}, \quad (5b)$$

$$\Psi'_{EI}|_{x=0^+} - \Psi'_{SM}|_{x=0^-} = \mathcal{M}_1 \Psi_{SM}|_{x=0}, \quad (5c)$$

$$\Psi'_S|_{x=L^+} - \Psi'_{EI}|_{x=L^-} = \mathcal{M}_2 \Psi_{EI}|_{x=L}, \quad (5d)$$

where $\mathcal{M}_{1(2)} = k_0 Z_{1(2)} \tau_0 \otimes \sigma_z$, with τ_0 a 2×2 unit matrix operating in the Nambu space. Resorting to Eqs. (2)–(5), the reflection amplitudes can be obtained to define the reflection probabilities

$$R_{qe}^{\alpha T} = \left| \frac{\langle \psi_{SM,q}^{\alpha,-} | \hat{j}_x | \psi_{SM,q}^{\alpha,-} \rangle}{\langle \psi_{SM,e}^{T,+} | \hat{j}_x | \psi_{SM,e}^{T,+} \rangle} \right| |r_{qe}^{\alpha T}|^2, \quad (6)$$

where $\alpha = T(B)$ labels the top (bottom) layer, $q = e(h)$ denotes the electron (hole), and the particle current density operator $\hat{j}_x \equiv -\frac{i}{\hbar} [x, \mathcal{H}] = -i \frac{\hbar}{m} \partial_x \tau_z \otimes \sigma_z$.

Taking advantage of the reflection probabilities, the differential shot noise at zero temperature can be obtained in accordance with the Landauer formula [46],

$$\begin{aligned} S(E) = 2eG_0 \int_0^{\frac{\pi}{2}} & [(R_{he}^{TT} + R_{he}^{BT})(1 - R_{he}^{TT} - R_{he}^{BT}) \\ & + (R_{ee}^{TT} + R_{ee}^{BT})(1 - R_{ee}^{TT} - R_{ee}^{BT}) + 2(R_{he}^{TT} + R_{he}^{BT}) \\ & \times (R_{ee}^{TT} + R_{ee}^{BT})] \cos \theta d\theta, \end{aligned} \quad (7)$$

where $G_0 = \frac{2e^2}{h} \frac{W \sqrt{2m(\mathcal{E}+E)}}{\pi \hbar}$ indicates the differential conductance of the normal state, E is the incident energy, and $\theta = \sin^{-1}(\frac{\hbar k_y}{\sqrt{2m(\mathcal{E}+E)}})$ denotes the incident angle. The mathematical details concerning the derivation of Eq. (7) are given in Appendix B. Accordingly, the noise-to-current ratio, i.e., the

Fano factor, can be expressed as [46]

$$F = \frac{\int_0^{eV} S(E) dE}{2e \int_0^{eV} G(E) dE}, \quad (8)$$

where $G(E) = G_0 \int_0^{\pi/2} (1 + R_{he}^{TT} + R_{he}^{BT} - R_{ee}^{TT} - R_{ee}^{BT}) \cos \theta d\theta$ denotes the differential conductance of the SM-EI-S junction, and V parametrizes the bias voltage.

III. RESULTS AND DISCUSSION

In this section, we perform the numerical calculation and illustrate the manifestations of the exciton condensate in the nonequilibrium current fluctuations. In the numerical calculation, $\Delta = 4\Gamma$ and $\mathcal{E} = 100\Gamma$ are fixed for definiteness, and the length of EI region L is set in units of the exciton coherence length $\xi_\Gamma = \hbar^2 k_0 / (m\Gamma)$ [29,30]. To address the effects of the exciton-mediated scattering on the nonequilibrium current fluctuations, we compare the scenarios in a SM-EI-S junction with exciton condensates (i.e., with a finite EI region of length $L \neq 0$) to those of a SM-S junction without exciton condensates (i.e., without the EI region by setting $L = 0$).

As a starting point, we concentrate on the differential shot noise in a well-contacted SM-EI-S junction with $Z_1 = Z_2 = 0$. In the situation of $L = 0$, the exciton-mediated interlayer scattering processes disappear and only the intralayer NR and intralayer AR processes contribute to the transport. Since the junction is well contacted with $Z_1 = Z_2 = 0$, for $0 < E < \Delta$ the intralayer AR process dominates over the intralayer NR process [26,51], strongly suppressing the randomness of scattering. Consequently, the differential shot noise almost vanishes in the regime of $0 < E < \Delta$, as indicated by the solid curve in Fig. 2(a). In the presence of exciton condensate, i.e., $L \neq 0$, the differential shot noise emerges and is highly sensitive to the incident energy E , in stark contrast to the case of $L = 0$. Remarkably, when $L \geq \xi_\Gamma$ to sufficiently prohibit the direct tunneling of evanescent modes, the profile of E -dependent differential shot noise exhibits a minimum at $E \simeq \Gamma$, as depicted in Fig. 2(a). This phenomenon can be ascribed to the energy-dependent competition between the exciton-mediated interlayer NR and the Cooper-pair-mediated intralayer AR in the regime of $0 < E < \Delta$. Specifically, in the case of $E \simeq 0$ the intralayer AR probability keeps finite since the contacts are ideal with $Z_1 = Z_2 = 0$ [26], although the exciton-mediated interlayer NR arises. As a consequence, at $E \simeq 0$ the coexistence of intralayer AR and interlayer NR processes results in the randomness of scattering and enables the differential shot noise to be finite. As E increases up to Γ , the exciton-mediated interlayer NR process dominates over the intralayer AR process and profoundly suppresses the randomness of the scattering, leading to the reduction of the differential shot noise. By further increasing E into the regime of $\Gamma < E < \Delta$, the particles with $|k_y| < \sqrt{2m(\mathcal{E} \pm \sqrt{E^2 - \Gamma^2})}/\hbar$ can propagate across the EI region to participate in the AR process. When E is just over Γ the scattering is random because the retrieved intralayer AR probability is comparable to the interlayer NR probability, while by further increasing E up to Δ the intralayer AR process becomes dominant and suppresses the scattering randomness again [26]. Therefore, in the case of $\Gamma < E < \Delta$

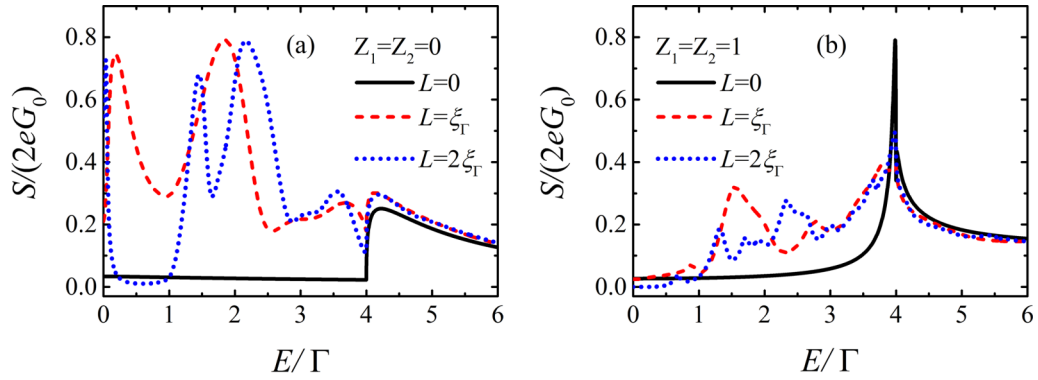


FIG. 2. The differential shot noise S as a function of the incident energy E in (a) a well-contacted SM-EI-S junction with $Z_1 = Z_2 = 0$ and (b) a tunnel SM-EI-S junction with $Z_1 = Z_2 = 1$, where $\Delta = 4\Gamma$.

the differential shot noise initially increases and then decays by enhancing the incident energy. By comparing the scenarios related to $L = 0$ and $L \neq 0$, we conclude that, in addition to the differential conductance proposed in Refs. [26,27], the differential shot noise spectroscopy can also be utilized to identify the existence of exciton condensate in a well-contacted SM-EI-S junction.

We now turn to the differential shot noise in a tunnel SM-EI-S junction with $Z_1 = Z_2 = 1$. An immediate consequence of the interfacial potential barriers is the suppression of the AR process at $E \simeq 0$ (see Fig. 3), resulting in the disappearance of the zero-energy conductance peak [51]. Therefore, differing from that in a well-contacted SM-EI-S junction [26,27], in a tunnel SM-EI-S junction the minimum of differential conductance caused by the exciton condensate

becomes ambiguous. In contrast, as charted out in Fig. 2(b), the differential shot noises corresponding to $L = 0$ (without exciton condensates) and $L \neq 0$ (with exciton condensates) possess markedly distinct configurations. In this sense, we state that the differential shot noise can offer a distinguishable signature to probe the exciton condensate even in a tunnel SM-EI-S junction. On the other hand, the interfacial potential barriers can profoundly affect the interplay between the exciton-mediated NR and the Cooper-pair-mediated AR processes. To be more specific, we take the scenarios in a tunnel SM-EI-S junction with $L = \xi_\Gamma$ as examples and illustrate the underlying physics by virtue of the reflection probabilities shown in Fig. 3. In the case of $0 < E < \Gamma$, the incident particles are blocked by the excitonic gap and the interfacial potential barriers, thus both the intralayer AR and interlayer

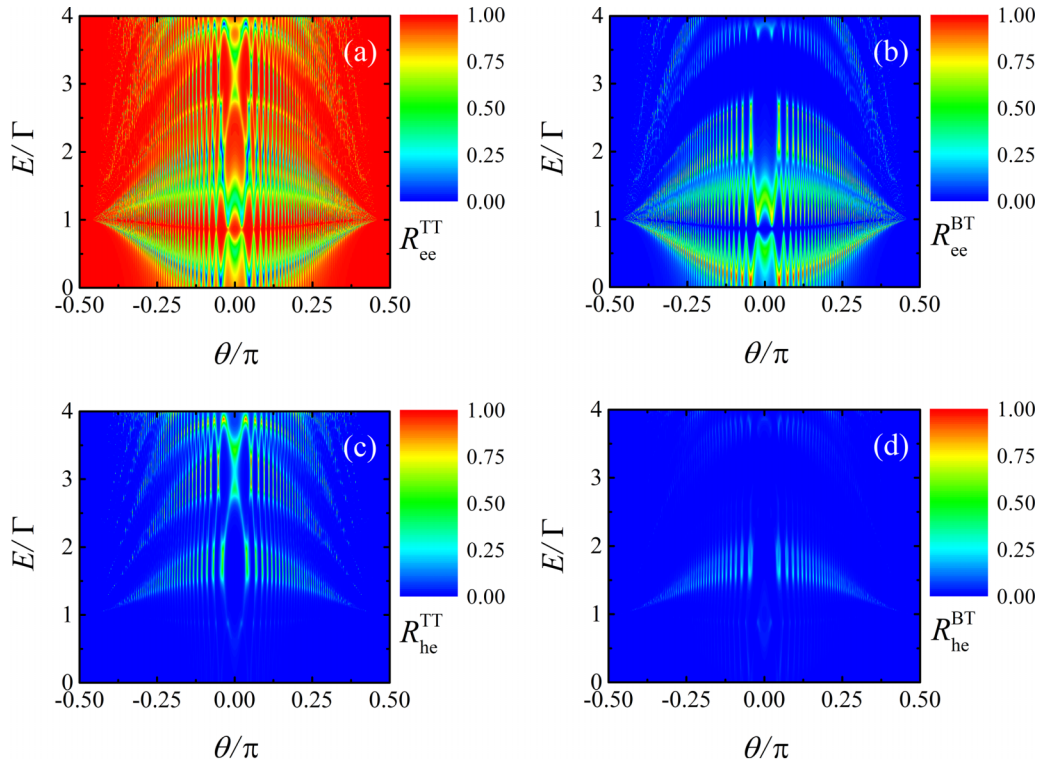


FIG. 3. Contour plots of the reflection probabilities of a tunnel SM-EI-S junction versus the incident angle θ and the incident energy E , where $Z_1 = Z_2 = 1$, $L = \xi_\Gamma$, and $\Delta = 4\Gamma$.

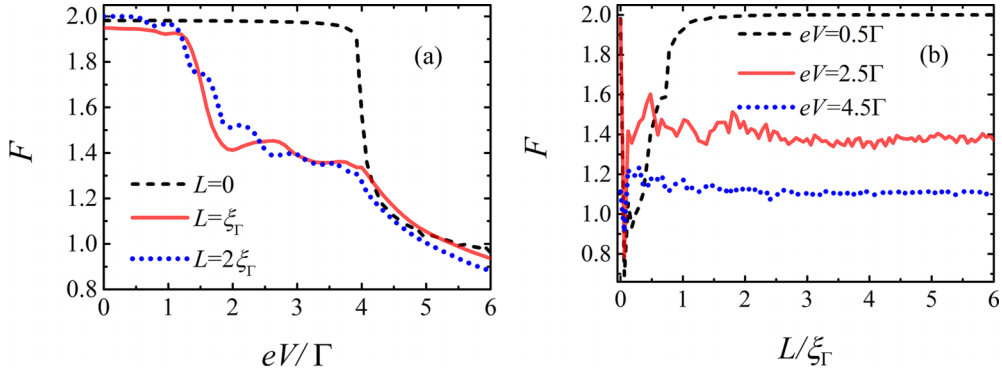


FIG. 4. The Fano factor F of a tunnel SM-EI-S junction varies with (a) the bias voltage eV and (b) the length of the EI region L . In both panels, $Z_1 = Z_2 = 1$ and $\Delta = 4\Gamma$.

AR, are strongly suppressed, as depicted in Figs. 3(c) and 3(d). As a result, the differential shot noise almost vanishes in the regime of $0 < E < \Gamma$, as shown in Fig. 2(b). When $E > \Gamma$, however, propagating modes emerge in the EI region and which can in turn reach the EI-S interface to participate in the AR processes, as indicated by the enhanced AR probabilities shown in Figs. 3(c) and 3(d). The presence of AR processes results in the randomness of scattering, leading to the enhancement of the differential shot noise shown in Fig. 2(b). Moreover, the two interfacial potential barriers enable the EI region to form a resonant double-barrier structure, thus in the case of $\Gamma < E < \Delta$ the E -dependent reflection probabilities exhibit pronounced resonance textures (see Fig. 3). This scattering configuration leads to the oscillating profile in the E -dependent differential shot noise when $\Gamma < E < \Delta$, as indicated by the short-dash and short-dot curves shown in Fig. 2(b).

To clarify the effect of exciton-mediated scattering on the charge transfer, we proceed to analyze the Fano factor F in a tunnel SM-EI-S junction with $Z_1 = Z_2 = 1$. We note that previous endeavors have demonstrated that in a NS junction the value of F in the subgap regime of $0 < eV < \Delta$ depends on the transparency of the N region [45,46]. Explicitly, in a NS junction with a low transparent N region the value of Fano factor is located within the super-Poissonian range of $1 < F < 2$, while for an opaque N region F tends to the value of two. Based on this general concept, we elucidate the scenarios of the Fano factor presented in Fig. 4(a). For $L = 0$, the exciton-mediated scattering disappears and only intralayer NR and intralayer AR processes are responsible for the subgap transport. Since the interfacial potential barrier strongly suppresses the transparency, F takes a constant value of two in the whole subgap regime of $0 < eV < \Delta$, which is consistent with the results in an opaque NS junction [45,46]. In a tunnel SM-EI-S junction with $L \neq 0$, the transparency, and thus the Fano factor, are profoundly influenced by the exciton-mediated scattering. In the case of $0 < eV < \Gamma$, owing to the blockade effects resulting from the interfacial potential barrier located at $x = 0$ and the excitonic gap of the EI region, the incident particles are mostly reflected back to the SM region, respectively, via the intralayer NR and the exciton-mediated interlayer NR processes (see the plots of R_{ee}^{TT} and R_{ee}^{BT} shown in Fig. 3). Consequently, as shown in Fig. 4(a), F keeps the value of two in the regime

of $0 < eV < \Gamma$. While for $\Gamma < eV < \Delta$, on the one hand, the particles with $|k_y| < \sqrt{2m(\mathcal{E} \pm \sqrt{(eV)^2 - \Gamma^2})/\hbar^2}$ can propagate through the EI region to improve the transparency, as evidenced by the apparent enhancements of R_{he}^{TT} and R_{he}^{BT} shown in Figs. 3(c) and 3(d), respectively. On the other hand, even in the case of $\Gamma < eV < \Delta$ the transparency of the EI region remains low, due to the strong intralayer NR [refer to Fig. 3(a)] dictated by the interfacial potential barriers. Therefore, in the regime of $\Gamma < eV < \Delta$ the Fano factor drops into the super-Poissonian range of $1 < F < 2$. By comparing the visibly distinct configurations of eV -dependent Fano factors corresponding to $L = 0$ and $L \neq 0$, we conclude that in a tunnel SM-EI-S junction the Fano factor can be taken as a fingerprint to signify the existence of exciton condensate. Moreover, as shown in Fig. 4(b), when L is large enough (normally several ξ_Γ) to sufficiently suppress the direct tunneling of evanescent modes, the value of F is weakly dependent on L . Practically, this means that when the length of the EI region is substantially longer than the exciton coherence length, the Fano factor is insensitive to the structural parameters of the SM-EI-S junction. This character renders the Fano factor favorable for the experimental detection of exciton condensate in a tunnel SM-EI-S junction.

IV. CONCLUSION

To conclude, we have theoretically studied the differential shot noise and the Fano factor in a SM-EI-S junction by virtue of the scattering wave approach. By comparing the corresponding scenarios in the SM-EI-S junctions with and without exciton condensates, we have illustrated the manifestations of exciton condensates in the differential shot noise and the Fano factor. In both well-contacted and tunnel SM-EI-S junctions, we have verified that the shot noise spectroscopy can be employed to identify the existence of exciton condensates, thus extending the previous proposals on the charge transport measurements of neutral exciton condensates to the situations of tunnel SM-EI-S junctions. We have shown that, as a consequence of the competition between the exciton-mediated intralayer NR and the Cooper-pair-mediated intralayer AR, the Fano factor in a tunnel SM-EI-S junction lies in the super-Poissonian regime when $\Gamma < eV < \Delta$. Taking advantage of the scattering probabilities, we have explicitly elucidated the underlying physics. Furthermore, we have revealed that when

the junction length is large enough to sufficiently prohibit the direct tunneling of evanescent modes, the value of the Fano factor in a tunnel SM-EI-S junction is insensitive to the geometrical parameters. These findings offer a feasible route for probing the neutral exciton condensate in bilayer systems through charge transport measurements. We anticipate more interesting results on the exciton-mediated nonequilibrium current fluctuations in multiterminal EI-based superconducting hybrid junctions.

ACKNOWLEDGMENTS

This work was supported by the Foundation of Hunan Educational Committee (Grants No. 23A0086 and No. 18B014), the Science and Technology Planning Project of Hunan Province (Grant No. 2019RS2033), the National Natural Science Foundation of China (Grant No. 11804091), and the Hunan Provincial Natural Science Foundation (Grant No. 2019JJ50380).

APPENDIX A: CALCULATION OF THE BASIS SCATTERING STATES IN A SM-EI-S JUNCTION

In this Appendix we present necessary calculation details regarding the basis scattering states in a SM-EI-S junction.

We assume that the translational symmetry is preserved in the y direction, so that the transverse momentum k_y can be taken as a good quantum number. By solving the eigenvalue equation $\mathcal{H}(-i\partial_x, k_y)\psi = E\psi$ straightforwardly, the related basis scattering states in the SM region ($x < 0$) can be formulated as

$$\psi_{SM,e(h)}^{T(B),\pm} = \hat{e}_{1(4)} e^{\pm i\kappa_+ x + ik_y y}, \quad (A1a)$$

$$\psi_{SM,e(h)}^{B(T),-} = \hat{e}_{2(3)} e^{i\kappa_- x + ik_y y}, \quad (A1b)$$

where $\kappa_{\pm} = \sqrt{2m(\mathcal{E} \pm E)/\hbar^2 - k_y^2}$, $\hat{e}_1 = [1, 0, 0, 0]^T$, $\hat{e}_2 = [0, 1, 0, 0]^T$, $\hat{e}_3 = [0, 0, 1, 0]^T$, $\hat{e}_4 = [0, 0, 0, 1]^T$, and \mathcal{T} denotes the transpose operation.

In the S region ($x > L$), the involved basis scattering states are given by

$$\psi_{S,\tilde{e}(\tilde{h})}^{T(B),+} = [\tilde{u}\hat{e}_{1(4)} + \tilde{v}\hat{e}_{3(2)}] e^{i\tilde{\kappa}_+ x + ik_y y}, \quad (A2a)$$

$$\psi_{S,\tilde{e}(\tilde{h})}^{B(T),+} = [\tilde{u}\hat{e}_{2(3)} + \tilde{v}\hat{e}_{4(1)}] e^{-i\tilde{\kappa}_- x + ik_y y}, \quad (A2b)$$

with related parameters being defined as $\tilde{u}(\tilde{v}) = \sqrt{[1 + (-)\sqrt{1 - \Delta^2/E^2}]/2}$ and $\tilde{\kappa}_{\pm} = \sqrt{2m(\mathcal{E} \pm \sqrt{E^2 - \Delta^2})/\hbar^2 - k_y^2}$.

In the EI region of $0 < x < L$, the counter-propagating scattering states can be expressed as

$$\psi_{EI,e(h)}^{T(B),\pm} = [u\hat{e}_{1(4)} + v\hat{e}_{2(3)}] e^{\pm i\kappa_+ x + ik_y y}, \quad (A3a)$$

$$\psi_{EI,h(e)}^{T(B),\pm} = [u\hat{e}_{3(2)} + v\hat{e}_{4(1)}] e^{\mp i\kappa_- x + ik_y y}, \quad (A3b)$$

where $u(v) = \sqrt{[1 + (-)\sqrt{1 - \Gamma^2/E^2}]/2}$ and $k_{\pm} = \sqrt{2m(\mathcal{E} \pm \sqrt{E^2 - \Gamma^2})/\hbar^2 - k_y^2}$.

APPENDIX B: DERIVATION OF THE SHOT NOISE IN A SM-EI-S JUNCTION

To calculate the shot noise in the present setup, we extend the related formula developed in Ref. [42] to the sublayer space. In the zero-frequency limit, the current fluctuation spectral function between contacts i and j can be expressed as [42,46]

$$\begin{aligned} \langle \Delta I_i \Delta I_j \rangle &= \frac{2e^2}{h} \sum_{\rho,\sigma,\mu,\nu \in \{T,B\}} \sum_{\alpha,\beta,\gamma,\delta \in \{e,h\}} \sum_{k,l \in \{N,S\}} \text{sgn}(\alpha)\text{sgn}(\beta) \\ &\times \int dEA_{k\gamma\mu;l\delta\nu}(i\alpha\rho, E) A_{l\delta\nu;k\gamma\mu}(j\beta\sigma, E) f_{k\gamma}(E) \\ &\times [1 - f_{l\delta}(E)], \end{aligned} \quad (B1)$$

where the indices $i, j \in \{N, S\}$ denote the nonsuperconducting or superconducting terminal, $\text{sgn}(\alpha) = +(-)1$ for $\alpha = e(h)$ labels the sign of contribution from an electron (a hole), $f_{k\gamma}(E) = 1/[1 + \exp[(E - \text{sgn}(\gamma)E_{F,k})/(k_B T_k)]]$ is the Fermi-Dirac distribution function for a particle of type γ in contact k , with k_B the Boltzmann constant, T_k the temperature in contact k , and $E_{F,k}$ the chemical potential of contact k . The parameter $A_{k\gamma\mu;l\delta\nu}(i\alpha\rho, E)$ is given by

$$A_{k\gamma\mu;l\delta\nu}(i\alpha\rho, E) = \delta_{ik}\delta_{il}\delta_{\alpha\gamma}\delta_{\alpha\delta}\delta_{\rho\mu}\delta_{\rho\nu} - s_{ik}^{\alpha\gamma,\rho\mu\dagger} s_{il}^{\alpha\delta,\rho\nu}, \quad (B2)$$

where δ_{mn} with $\{mn\} \in \{ik, il, \alpha\gamma, \alpha\delta, \rho\mu, \rho\nu\}$ as the Kronecker delta, and $s_{ik}^{\alpha\gamma,\rho\mu}$ as the scattering matrix element, labeling the scattering amplitude for a particle of type γ stemming from the layer μ of contact k scattered to the layer ρ of contact i as a particle of type α .

In the zero-temperature limit, the current fluctuation spectral function contains only the nonequilibrium part, i.e., the shot noise power \mathcal{S}_{ij} . Accordingly, at zero-temperature the local shot noise power \mathcal{S}_{NN} measured in the nonsuperconducting terminal can be written as

$$\begin{aligned} \mathcal{S}_{NN} &= \frac{4e^2}{h} \int_0^{eV} dE \{ T_{NN}^{ee,TT} (1 - T_{NN}^{ee,TT}) + T_{NN}^{ee,TB} (1 - T_{NN}^{ee,TB}) - 2T_{NN}^{ee,TT} T_{NN}^{ee,TB} \\ &+ T_{NN}^{ee,BT} (1 - T_{NN}^{ee,BT}) + T_{NN}^{ee,BB} (1 - T_{NN}^{ee,BB}) - 2T_{NN}^{ee,BT} T_{NN}^{ee,BB} \\ &+ T_{NN}^{he,TT} (1 - T_{NN}^{he,TT}) + T_{NN}^{he,TB} (1 - T_{NN}^{he,TB}) - 2T_{NN}^{he,TT} T_{NN}^{he,TB} \\ &+ T_{NN}^{he,BT} (1 - T_{NN}^{he,BT}) + T_{NN}^{he,BB} (1 - T_{NN}^{he,BB}) - 2T_{NN}^{he,BT} T_{NN}^{he,BB} \\ &+ T_{NN}^{ee,TT} T_{NN}^{he,TT} + T_{NN}^{ee,TB} T_{NN}^{he,TB} + s_{NN}^{ee,TB\dagger} s_{NN}^{he,TT} s_{NN}^{he,TT\dagger} s_{NN}^{he,TB} + s_{NN}^{ee,TT\dagger} s_{NN}^{ee,TB} s_{NN}^{he,TB\dagger} s_{NN}^{he,TT} \\ &+ T_{NN}^{he,TT} T_{NN}^{ee,TT} + T_{NN}^{he,TB} T_{NN}^{ee,TB} + s_{NN}^{he,TB\dagger} s_{NN}^{he,TT} s_{NN}^{ee,TT\dagger} s_{NN}^{ee,TB} + s_{NN}^{he,TT\dagger} s_{NN}^{he,TB} s_{NN}^{ee,TB\dagger} s_{NN}^{ee,TT} \} \end{aligned}$$

$$\begin{aligned}
 & + T_{NN}^{ee,BT} T_{NN}^{he,BT} + T_{NN}^{ee,BB} T_{NN}^{he,BB} + s_{NN}^{ee,BB\dagger} s_{NN}^{ee,BT} s_{NN}^{he,BT\dagger} s_{NN}^{he,BB} + s_{NN}^{ee,BT\dagger} s_{NN}^{ee,BB} s_{NN}^{he,BB\dagger} s_{NN}^{he,BT} \\
 & + T_{NN}^{he,BT} T_{NN}^{ee,BT} + T_{NN}^{he,BB} T_{NN}^{ee,BB} + s_{NN}^{he,BB\dagger} s_{NN}^{he,BT} s_{NN}^{ee,BT\dagger} s_{NN}^{ee,BB} + s_{NN}^{he,BT\dagger} s_{NN}^{he,BB} s_{NN}^{ee,BB\dagger} s_{NN}^{ee,BT} \\
 & - T_{NN}^{ee,TT} T_{NN}^{ee,BT} - T_{NN}^{ee,TB} T_{NN}^{ee,BB} - s_{NN}^{ee,TT\dagger} s_{NN}^{ee,TB} s_{NN}^{ee,BB\dagger} s_{NN}^{ee,BT} - s_{NN}^{ee,TB\dagger} s_{NN}^{ee,TT} s_{NN}^{ee,BT\dagger} s_{NN}^{ee,BB} \\
 & - T_{NN}^{ee,BT} T_{NN}^{ee,TT} - T_{NN}^{ee,BB} T_{NN}^{ee,TB} - s_{NN}^{ee,BT\dagger} s_{NN}^{ee,BB} s_{NN}^{ee,TB\dagger} s_{NN}^{ee,TT} - s_{NN}^{ee,BB\dagger} s_{NN}^{ee,BT} s_{NN}^{ee,TT\dagger} s_{NN}^{ee,TB} \\
 & - T_{NN}^{he,TT} T_{NN}^{he,BT} - T_{NN}^{he,TB} T_{NN}^{he,BB} - s_{NN}^{he,TT\dagger} s_{NN}^{he,TB} s_{NN}^{he,BB\dagger} s_{NN}^{he,BT} - s_{NN}^{he,TB\dagger} s_{NN}^{he,TT} s_{NN}^{he,BT\dagger} s_{NN}^{he,BB} \\
 & - T_{NN}^{he,BT} T_{NN}^{he,TT} - T_{NN}^{he,BB} T_{NN}^{he,TB} - s_{NN}^{he,BT\dagger} s_{NN}^{he,BB} s_{NN}^{he,TB\dagger} s_{NN}^{he,TT} - s_{NN}^{he,BB\dagger} s_{NN}^{he,BT} s_{NN}^{he,TT\dagger} s_{NN}^{he,TB} \\
 & + T_{NN}^{ee,TT} T_{NN}^{he,BT} + T_{NN}^{ee,TB} T_{NN}^{he,BB} + s_{NN}^{ee,TT\dagger} s_{NN}^{ee,TB} s_{NN}^{he,BB\dagger} s_{NN}^{he,BT} + s_{NN}^{ee,TB\dagger} s_{NN}^{ee,TT} s_{NN}^{he,BT\dagger} s_{NN}^{he,BB} \\
 & + T_{NN}^{he,BT} T_{NN}^{he,TT} + T_{NN}^{ee,BB} T_{NN}^{he,TB} + s_{NN}^{ee,BT\dagger} s_{NN}^{ee,BB} s_{NN}^{he,TB\dagger} s_{NN}^{he,TT} + s_{NN}^{ee,BB\dagger} s_{NN}^{ee,BT} s_{NN}^{he,TT\dagger} s_{NN}^{he,TB} \\
 & + T_{NN}^{he,TT} T_{NN}^{ee,BT} + T_{NN}^{he,TB} T_{NN}^{ee,BB} + s_{NN}^{he,TT\dagger} s_{NN}^{he,BT} s_{NN}^{ee,BB\dagger} s_{NN}^{ee,BT} + s_{NN}^{he,TB\dagger} s_{NN}^{he,TT} s_{NN}^{ee,BT\dagger} s_{NN}^{ee,BB} \\
 & + T_{NN}^{he,BT} T_{NN}^{ee,TT} + T_{NN}^{he,BB} T_{NN}^{ee,TB} + s_{NN}^{he,BT\dagger} s_{NN}^{he,BB} s_{NN}^{ee,TB\dagger} s_{NN}^{ee,TT} + s_{NN}^{he,BB\dagger} s_{NN}^{he,BT} s_{NN}^{ee,TT\dagger} s_{NN}^{ee,TB} \}. \tag{B3}
 \end{aligned}$$

where the scattering probabilities $T_{ik}^{\alpha\gamma,\rho\mu} = |s_{ik}^{\alpha\gamma,\rho\mu}|^2$. Taking advantage of Eq. (B3), the differential shot noise can be formulated as

$$S(E) = \frac{\partial \mathcal{S}_{NN}}{\partial V}, \tag{B4}$$

with V the bias voltage. In a SM-EI-S junction, for the scattering scenarios caused by an electron incident from the top layer of the SM region, the differential shot noise given by Eq. (B4) can be simplified straightforwardly to the form shown in Eq. (7).

- [1] D. Jérôme, T. M. Rice, and W. Kohn, Excitonic insulator, *Phys. Rev.* **158**, 462 (1967).
- [2] D. V. Fil and S. I. Shevchenko, Electron-hole superconductivity (review), *Low Temp. Phys.* **44**, 867 (2018).
- [3] B. I. Halperin and T. M. Rice, Possible anomalies at a semimetal-semiconductor transition, *Rev. Mod. Phys.* **40**, 755 (1968).
- [4] A. Kogar, M. S. Rak, S. Vig, A. A. Husain, F. Flicker, Y. I. Joe, L. Venema, G. J. MacDougall, T. C. Chiang, E. Fradkin, J. van Wezel, and P. Abbamonte, Signatures of exciton condensation in a transition metal dichalcogenide, *Science* **358**, 1314 (2017).
- [5] H. Ning, O. Mehio, M. Buchhold, T. Kurumaji, G. Refael, J. G. Checkelsky, and D. Hsieh, Signatures of ultrafast reversal of excitonic order in Ta₂NiSe₅, *Phys. Rev. Lett.* **125**, 267602 (2020).
- [6] Y. F. Lu, H. Kono, T. I. Larkin, A. W. Rost, T. Takayama, A. V. Boris, B. Keimer, and H. Takagi, Zero-gap semiconductor to excitonic insulator transition in Ta₂NiSe₅, *Nat. Commun.* **8**, 14408 (2017).
- [7] P. Wang, G. Yu, Y. Jia, M. Onyszczak, F. A. Cevallos, S. Lei, S. Klemenz, K. Watanabe, T. Taniguchi, R. J. Cava, L. M. Schoop, and S. Wu, Landau quantization and highly mobile fermions in an insulator, *Nature (London)* **589**, 225 (2021).
- [8] B. Sun, W. Zhao, T. Palomaki, Z. Fei, E. Runburg, P. Malinowski, X. Huang, J. Cenker, Y.-T. Cui, J.-H. Chu, X. Xu, S. S. Ataei, D. Varsano, M. Palummo, E. Molinari, M. Rontani, and D. H. Cobden, Evidence for equilibrium exciton condensation in monolayer WTe₂, *Nat. Phys.* **18**, 94 (2022).
- [9] Z. Wang, D. A. Rhodes, K. Watanabe, T. Taniguchi, J. C. Hone, J. Shan, and K. F. Mak, Evidence of high-temperature exciton condensation in two-dimensional atomic double layers, *Nature (London)* **574**, 76 (2019).
- [10] L. Ma, P. X. Nguyen, Z. Wang, Y. Zeng, K. Watanabe, T. Taniguchi, A. H. MacDonald, K. F. Mak, and J. Shan, Strongly correlated excitonic insulator in atomic double layers, *Nature (London)* **598**, 585 (2021).
- [11] J. Gu, L. Ma, S. Liu, K. Watanabe, T. Taniguchi, J. C. Hone, J. Shan, and K. F. Mak, Dipolar excitonic insulator in a moiré lattice, *Nat. Phys.* **18**, 395 (2022).
- [12] R. Xiong, J. H. Nie, S. L. Brantly, P. Hays, R. Sailus, K. Watanabe, T. Taniguchi, S. Tongay, and C. Jin, Correlated insulator of excitons in WSe₂/WS₂ moiré superlattices, *Science* **380**, 860 (2023).
- [13] R. Wang, T. A. Sedrakyan, B. Wang, L. Du, and R.-R. Du, Excitonic topological order in imbalanced electron-hole bilayers, *Nature (London)* **619**, 57 (2023).
- [14] Y. Zeng, Z. Xia, R. Dery, K. Watanabe, T. Taniguchi, J. Shan, and K. F. Mak, Exciton density waves in Coulomb-coupled dual moiré lattices, *Nat. Mater.* **22**, 175 (2023).
- [15] Z. Sun, T. Kaneko, D. Golež, and A. J. Millis, Second-order josephson effect in excitonic insulators, *Phys. Rev. Lett.* **127**, 127702 (2021).
- [16] Y.-F. Hsu and J.-J. Su, Single interface effects dominate in exciton-condensate/normal-barrier/exciton-condensate (EC/N/EC) structures of long-barrier, *New J. Phys.* **20**, 083002 (2018).
- [17] C. Zhang, W. Zhang, Y. Jia, and Z. Zhang, Sustaining charge-neutral or charged supercurrents in excitonic josephson junctions based on graphene heterostructures, *Phys. Rev. B* **104**, 195309 (2021).

- [18] D. Zhang, J. Falson, S. Schmult, W. Dietsche, and J. H. Smet, Quasiparticle tunneling across an exciton condensate, *Phys. Rev. Lett.* **124**, 246801 (2020).
- [19] G. Sethi, Y. Zhou, L. Zhu, L. Yang, and F. Liu, Flat-band-enabled triplet excitonic insulator in a diatomic kagome lattice, *Phys. Rev. Lett.* **126**, 196403 (2021).
- [20] H. D. Scammell and O. P. Sushkov, Exciton condensation in biased bilayer graphene, *Phys. Rev. Res.* **5**, 043176 (2023).
- [21] M. Rontani and L. J. Sham, Coherent transport in a homojunction between an excitonic insulator and semimetal, *Phys. Rev. Lett.* **94**, 186404 (2005).
- [22] M. Rontani and L. J. Sham, Variable resistance at the boundary between semimetal and excitonic insulator, *Solid State Commun.* **134**, 89 (2005).
- [23] B. Wang, J. Peng, D. Y. Xing, and J. Wang, Spin current due to spinlike andreev reflection, *Phys. Rev. Lett.* **95**, 086608 (2005).
- [24] M. Veldhorst, M. Hoek, M. Snelder, H. Hilgenkamp, A. A. Golubov, and A. Brinkman, Nonlocal spin-entangled andreev reflection, fractional charge, and current-phase relations in topological bilayer-exciton-condensate junctions, *Phys. Rev. B* **90**, 035428 (2014).
- [25] A. D. K. Finck, J. P. Eisenstein, L. N. Pfeiffer, and K. W. West, Exciton transport and andreev reflection in a bilayer quantum hall system, *Phys. Rev. Lett.* **106**, 236807 (2011).
- [26] D. Bercioux, T. M. Klapwijk, and F. S. Bergeret, Transport properties of an electron-hole bilayer in contact with a superconductor hybrid junction, *Phys. Rev. Lett.* **119**, 067001 (2017).
- [27] D. Bercioux, B. Bujnowski, and F. S. Bergeret, Quantum transport properties of an exciton insulator/superconductor hybrid junction, *Adv. Quantum Technol.* **2**, 1800049 (2019).
- [28] A. Kononov, S. V. Egorov, Z. D. Kvon, N. N. Mikhailov, S. A. Dvoretzky, and E. V. Deviatov, Andreev reflection at the edge of a two-dimensional semimetal, *Phys. Rev. B* **93**, 041303(R) (2016).
- [29] F. Dolcini, D. Rainis, F. Taddei, M. Polini, R. Fazio, and A. H. MacDonald, Blockade and counterflow supercurrent in exciton-condensate josephson junctions, *Phys. Rev. Lett.* **104**, 027004 (2010).
- [30] S. Peotta, M. Gibertini, F. Dolcini, F. Taddei, M. Polini, L. B. Ioffe, R. Fazio, and A. H. MacDonald, Josephson current in a four-terminal superconductor/exciton-condensate/superconductor system, *Phys. Rev. B* **84**, 184528 (2011).
- [31] H. Soller, F. Dolcini, and A. Komnik, Nanotransformation and current fluctuations in exciton condensate junctions, *Phys. Rev. Lett.* **108**, 156401 (2012).
- [32] H. Soller, Exciton condensates and superconductors-technical differences and physical similarities, *J. Appl. Math. Phys.* **03**, 1218 (2015).
- [33] H. Soller and A. Komnik, Current noise and higher order fluctuations in semiconducting bilayer systems, *Fluct. Noise Lett.* **12**, 1340001 (2013).
- [34] J.-X. Zhu and C. S. Ting, Shot noise in a normal-metal- d -wave superconductor junction with a 110-oriented interface, *Phys. Rev. B* **59**, R14165 (1999).
- [35] P. Zhou, L. Chen, Y. Liu, I. Sochnikov, A. T. Bollinger, M.-G. Han, Y. Zhu, X. He, I. Božović, and D. Natelson, Electron pairing in the pseudogap state revealed by shot noise in copper oxide junctions, *Nature (London)* **572**, 493 (2019).
- [36] N. Walldorf, F. Brange, C. Padurariu, and C. Flindt, Noise and full counting statistics of a cooper pair splitter, *Phys. Rev. B* **101**, 205422 (2020).
- [37] M. W. Prestel, M. Strohmeier, W. Belzig, and E. Scheer, Revealing channel polarization of atomic contacts of ferromagnets and strong paramagnets by shot-noise measurements, *Phys. Rev. B* **104**, 115434 (2021).
- [38] Z. Cao, G. Zhang, H. Zhang, Y.-X. Liang, W.-X. He, K. He, and D. E. Liu, Differential current noise as an identifier of andreev bound states that induce nearly quantized conductance plateaus, *Phys. Rev. B* **108**, L121407 (2023).
- [39] C. Ostrove and L. Reichl, Positive cross-correlated shot noise and quasibound states in an NSNSN geometry, *Phys. Rev. B* **103**, 224518 (2021).
- [40] K. M. Bastiaans, D. Cho, T. Benschop, I. Battisti, Y. Huang, M. S. Golden, Q. Dong, Y. Jin, J. Zaanen, and M. P. Allan, Charge trapping and super-Poissonian noise centres in a cuprate superconductor, *Nat. Phys.* **14**, 1183 (2018).
- [41] K. M. Bastiaans, D. Chatzopoulos, J.-F. Ge, D. Cho, W. O. Tromp, J. M. van Ruitenbeek, M. H. Fischer, P. J. de Visser, D. J. Thoen, E. F. Driessen *et al.*, Direct evidence for cooper pairing without a spectral gap in a disordered superconductor above T_c , *Science* **374**, 608 (2021).
- [42] M. P. Anantram and S. Datta, Current fluctuations in mesoscopic systems with andreev scattering, *Phys. Rev. B* **53**, 16390 (1996).
- [43] K. Kobayashi and M. Hashisaka, Shot noise in mesoscopic systems: from single particles to quantum liquids, *J. Phys. Soc. Jpn.* **90**, 102001 (2021).
- [44] B. A. Muzykantskii and D. E. Khmelnitskii, Quantum shot noise in a normal-metal-superconductor point contact, *Phys. Rev. B* **50**, 3982 (1994).
- [45] M. J. M. de Jong and C. W. J. Beenakker, Doubled shot noise in disordered normal-metal-superconductor junctions, *Phys. Rev. B* **49**, 16070 (1994).
- [46] Y. Blanter and M. Büttiker, Shot noise in mesoscopic conductors, *Phys. Rep.* **336**, 1 (2000).
- [47] P. Buset, B. Lu, S. Tamura, and Y. Tanaka, Current fluctuations in unconventional superconductor junctions with impurity scattering, *Phys. Rev. B* **95**, 224502 (2017).
- [48] S. Banerjee, S. Ikegaya, and A. P. Schnyder, Anomalous fano factor as a signature of bogoliubov fermi surfaces, *Phys. Rev. Res.* **4**, L042049 (2022).
- [49] X. Jehl, M. Sanquer, R. Calemczuk, and D. Mailly, Detection of doubled shot noise in short normal-metal/ superconductor junctions, *Nature (London)* **405**, 50 (2000).
- [50] A. F. Andreev, The thermal conductivity of the intermediate state in superconductors, *Zh. Eksp. Teor. Fiz.* **46**, 1823 (1964) [*Sov. Phys. JETP* **19**, 1228 (1964)].
- [51] G. E. Blonder, M. Tinkham, and T. M. Klapwijk, Transition from metallic to tunneling regimes in superconducting microconstrictions: Excess current, charge imbalance, and supercurrent conversion, *Phys. Rev. B* **25**, 4515 (1982).
- [52] B. Pannetier and H. Courtois, Andreev Reflection and Proximity effect, *J. Low Temp. Phys.* **118**, 599 (2000).